Photoluminescence mapping of the strain induced in InP and GaAs substrates by SiN stripes etched from thin films grown under controlled mechanical stress

Solène Gérard, Merwan Mokhtari, Jean-Pierre Landesman, Christophe Levallois, Marc Fouchier, Erwine Pargon, Philippe Pagnod-Rossiaux, Francois Laruelle, Alain Moréac, Brahim Ahammou, et al.

Highlights

- Stress effects in InP and GaAs induced by SiNx stripes of different widths
- Stress mapping by photo-luminescence (degree of polarization)
- SiNx films grown under different built-in stress (tensile or compressive)
- Model : edge force concept, anisotropic deformation, stress relaxation
- Process control for thin films growth

Photoluminescence mapping of the strain induced in InP and GaAs substrates by SiN_x stripes etched from thin films grown under controlled mechanical stress

Solène Gérard[a,*], Merwan Mokhtari[a], Jean-Pierre Landesman[a], Christophe Levallois[b], Marc Fouchier[c], Erwine Pargon[c], Philippe Pagnod-Rossiaux[d], François Laruelle[d], Alain Moréac[a], Brahim Ahammou[a], Daniel T. Cassidy[e]

[a] *Univ Rennes, CNRS, IPR – UMR 6251, F-35000 Rennes, France*
[b] *Univ Rennes, INSA Rennes, CNRS, Institut FOTON—UMR 6082, F-35000 Rennes, France*
[c] *Univ Grenoble Alpes, CNRS, LTM – UMR 5129, F-38000 Grenoble, France*
[d] *3SP Technologies S.A.S, Route de Villejust, F-91625 Nozay, France*
[e] *McMaster University, Department of Engineering Physics, Hamilton, Ontario L8S 4L7, Canada*

Abstract

We measured the details of the strain/stress fields produced in GaAs(100) and InP(100) substrates by the presence of narrow dielectric stripes processed from thin films obtained by plasma-enhanced chemical vapor deposition with a residual and controlled built-in compressive or tensile stress. Micro-photoluminescence techniques were used, measuring either the spectral shift of the luminescence peak or the degree of polarization (DOP) of the spectrally integrated signal. These techniques provide additional information on the different parts of the strain tensor (isotropic and anisotropic). The anisotropic deformation was found to change with the magnitude and sign of the initial built-in stress, and also with the stripe width. Using an analytical model, we were able to determine accurately several physical parameters which describe the stress/strain situation. The localized stress at the edges, expressed within the edge force concept, is shown to follow the expected initial built-in stress and also a stress reduction when the stripe width is decreased. This is interpreted as an evidence of some strain relaxation occuring near the stripe edges. This relaxation also impacts the shape of the DOP curves near the edges. The other important conclusion is the observation that the strain does not return to an isotropic situation (as in the case of an infinite thin film) in the central part of the stripes, even if the widths of these stripes are large (100 μm). The analytical model is developped and explained step by step. This analytical model produces quantitative data that describe the different effects observed. These data can be very helpful in the design and optimization of photonic devices when the photo-elastic effect

*Corresponding author
Email address: Solene.Gerard@univ-rennes1.fr (Solène Gérard)

can be significant, such as waveguides. The μPL measurements coupled with the model can also provide feedback to allow better control of the process conditions of such thin film devices.

Keywords: Dielectric thin film, Silicon nitride, Mechanical stress, Photoluminescence, Edge force, Anisotropic strain, Edge relaxation

1. Introduction

Mechanical stress and strain have long been identified as important concerns in the design and fabrication of photonic devices. For example, Huang [1] investigated the effects of mechanical stress (due to thermal mismatch of different layers) on the performance of silicon ridge waveguides. Photoelasticity (strain-induced modification of the optical index) can result in mutlimode operation of nominally single mode waveguides, occurrence of birefringence, transition losses, ...[1]. Photoelasticity is strong in III-V semiconductors and, as noted, can have deleterious side effects. On the other hand, mechanical strain can help improve the performance of some photonic or optoelectronic devices through "strain engineering". Most semiconductor laser diodes nowadays include a strained quantum well in their active area to improve the optical performance [2]. To account for the effects of stress/strain on the performance of devices under consideration, one needs accurate models to describe stress/strain distributions. Such a model must be validated against some kind of measurement. This question was covered in the literature already more than a century ago in the paper by Stoney [3] who established the formula relating the magnitude of the biaxial stress present in a thin film grown onto a substrate to the substrate curvature. This is the starting point that authors working on the problem have considered. This model cannot really be used to account for the stress/strain distribution in photonic and more generally semiconductor devices subjected to the presence of thin films (such as dielectrics) on their surface because these thin films are structured, parallel to the substrate surface, to dimensions sometimes less than a micron. Therefore the assumption of an infinite thin film does not hold. This point was taken into account through the development of the "edge force" model which was introduced in particular by Hu [4]. The basis of this model is that the discontinuity in the thin film can be treated as a line force, applied at the substrate surface along the discontinuity, which induces a deformation within the substrate and which can be described analytically. The salient feature of the deformation field is the concentration of the stress/strain components near the line of application of the force (in fact, within the framework of the analytical edge force model, this concentration appears as a mathematical divergence of the stress/strain components). This edge force model is one basis for the description of the physics of the deformation associated with thin films and coatings; see for example [5, 6]. The finite element simulation work performed by S.C. Jain et al. [7, 8] is another significant approach to this physics, which has shown in particular the importance of stress relaxation near the film edges, depending on the ratio of the film lateral dimension over film thickness. The

edge force model as well as the numerical simulation models predict that only areas in the substrate "close" to the film edges are significantly affected by the mechanical stress present in the thin film (how close will be addressed further in this paper). Therefore, when the impact of the edge force becomes negligible, the situation for the infinite film (i.e., biaxial stress in the film) should govern crystal deformation of the substrate. This is the question investigated in this article: how can the crystal deformation in a substrate under the influence of a structured thin film (for example a thin and narrow stripe) be described most accurately? We consider model devices, where a dielectric thin film is first grown on a semiconductor substrate (GaAs or InP) and then patterned in the shape of a thin and narrow stripe. The width of this stripe is a variable in our study. The effect that this stripe has on the underlying substrate is studied experimentally using micro-photoluminescence (μPL) with different approaches. The first approach is spectroscopic μPL, where the information on local strain is derived from the spectral shift [9]. The spectral shift of the μPL line informs us on the hydrostatic part of the crystal deformation, i.e., the volume change, when measured on a bulk semiconductor like GaAs or InP. The second experimental approach in this work uses the measurement of the degree of polarization (DOP) of the spectrally integrated μPL signal [10]. The DOP of μPL yields information on the anisotropic part of the crystal deformation below the dielectric stripe. The experimental information is then compared to the output of an analytical model. This model includes the edge force effect already described. In order to fit with the experimental data, it was necessary to add 2 other contributions to the edge force model: one corresponding to a residual anisotropic deformation below the central part of the stripes, far away from the edges, and another one related to a relaxation of the stress in the stripes close to their edges.

2. Samples and experiments

Figure 1 depicts the samples designed for this study. The stripes are made of silicon nitride SiN_x grown onto GaAs(100) and InP(100) n-doped substrates (with doping levels of the order of 10^{18} cm^{-3}) by plasma enhanced chemical vapor deposition (PECVD). Different PECVD reactors and different gas mixtures were used to grow the layers. Growth temperature for the SiN_x films was typically 250 to 300 °C. After deposition on full wafers, the films were patterned (by standard photo-lithography) and etched by reactive ion etching using a SF_6 or CF_4/O_2 plasma. The resulting stripes have different widths (along the x axis shown in fig. 1) from 3 to 100 μm. Their length (y axis in fig. 1) is typically 3 mm. Thickness of the SiN_x films was fixed for this study (500 nm).

During the PECVD process the SiN_x films are grown with a residual built-in stress which has 2 origins: thermal stress, and intrinsic stress due to ion bombarment effects in the PECVD reactor during growth of the film [11]. The built-in stress can be controlled through the operating parameters of the PECVD reactor (radio-frequency (RF) power, gas flows, total pressure). This stress was measured immediately after PECVD growth by the wafer curvature method

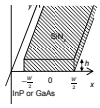

Figure 1: Geometry of a SiN_x stripe on an InP or GaAs (100) surface. W is the width of the stripe (centered at $x = 0$), and h its thickness.

[12]. An example of the evolution of the residual built-in stress versus power at the plasma source is shown in figure 2.

While the overall strain is obtained from the measurement of the full wafer curvature after thin film deposition, the local strain measurements are done by scanning the sample surface, across ridges with variable width, with a red laser beam (633 or 635 nm) focussed through a microscope objective (power density at the sample surface: $\sim$ kW·cm^{-2}). The step size is typically between 0.1 and 0.5 μm. The μPL signal is collected in a reverse geometry through the same microscope objective, and transferred to a grating spectrometer for the spectroscopic measurements or to a polarization analyzing system for the DOP measurements. For the spectroscopic measurements a commercial system is used. Details on the experimental procedure for the spectroscopic measurements of the hydrostatic strain can be found in [13]. We refer to [10, 14] for details on the DOP technique which provides measurements and mappings of the anisotropic component of the strain. The DOP technique uses the fact that the spectrally integrated PL signal from a bulk semiconductor like GaAs or InP, while unpolarized when the material is stress-free because of the cubic symmetry, becomes slightly polarized when the crystal is strained in such a way that the cubic symmetry is lost [15].

3. Experimental results

3.1. μPL spectral shift

Figure 3 shows the spectral shift of the PL line recorded while scanning the laser beam across the surface of InP(100) samples in areas with stripes of different widths W from 3 to 100 μm. In this case the SiN_x layer was grown with the minimum compressive stress (cf Figure 2), which is -30 MPa. To allow for an easier visualization, we have superimposed the curves for the different stripe widths on a single figure, choosing a logarithmic scale for the position x of the laser spot across the stripes. For each stripe, the part corresponding to negative x values has been folded onto the part for positive x values.

As indicated in [9, 13], the spectral shift of the μPL signal (for bulk semiconductors like GaAs or InP) can be considered in a first approximation as an estimation of the hydrostatic stress. According to Neuberger [16] for InP, a hydrostatic strain changes the energy gap following the equation
$\Delta E_G = -6.15 \cdot (\epsilon_{xx} + \epsilon_{yy} + \epsilon_{zz})$ eV which converts to
$\Delta\lambda = 3780 \cdot (\epsilon_{xx} + \epsilon_{yy} + \epsilon_{zz})$ nm.
A negative shift of 2 nm, as seen in fig. 3, thus indicates a compressive volume change $(\epsilon_{xx} + \epsilon_{yy} + \epsilon_{zz})$ of approximately 5×10^{-4} in the depth probed by the μPL signal. The absorption depth of InP at 633 nm is in the order of 150 nm [17]. The shifts measured below the SiN_x stripes in fig. 3 show a decreasing trend, from almost –2.5 nm ($W = 100\,\mu$m) to –1.5 nm ($W = 3\,\mu$m).
μPL spectral shifts were also measured for stripes with a fixed width, obtained from films grown under different built-in stresses, as illustrated in fig. 4 for GaAs.

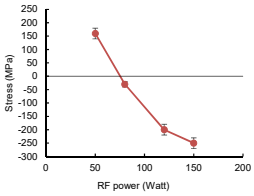

Figure 2: Built-in strain for the different SiN_x layers grown on InP(100), measured from wafer curvature. Precursor gas: $SiH_4/NH_3/N_2/Ar$; deposition temperature: 280 °C.

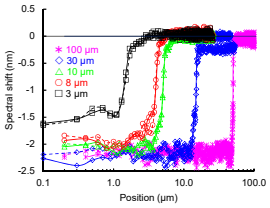

Figure 3: Spectral shift of the μPL for the SiN_x layer grown on InP(100) with minimum compressive stress (-30 MPa), and stripes with different widths. Pink curve with $*$: $W = 100\,\mu$m; blue curve with $\Diamond$: $W = 30\,\mu$m; green curve with $\triangle$: $W = 10\,\mu$m; red curve with $\bigcirc$: $W = 8\,\mu$m; black curve with $\square$: $W = 3\,\mu$m. For each curve, the full line indicates the measurements with positive x values, while the dash line indicates the folded part for negative x values.

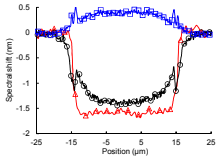

Figure 4: Spectral shifts of the μPL for compressive SiN_x layers on GaAs(100), and stripe width 30 μm. Black curve with ◯: high compressive stress (-250 MPa); red curve with △: low compressive stress (-10 MPa); blue curve with □: tensile stress (60 MPa).

We first observe the general trend that films with a compressive built-in stress yield a compressive spectral shift, whereas films with tensile built-in stress yield a tensile spectral shift. However, the magnitude of the spectral shift for the tensile film (60 MPa) is lower than the magnitude for the compressive films. Moreover, for the film with higher compressive built-in stress, sharp negative peaks in the spectral shift appear at the stripe edges. Also, comparing the two films with compressive built-in stress, one can see a different trend in the central part of the curve. While the curve for the (−10 MPa) film is flat, the curve for the (−250 MPa) film displays a reduced magnitude of the shift towards the edges. This could be interpreted as a partial relaxation of the volume compression. In fact the spectral shift measured for the (−10 MPa) film is higher – in magnitude – than the one measured for the (−250 MPa), which we cannot really explain at this point.

Other spectral shift measurements produced very noisy curves. It was difficult even to identify a trend on these curves. We think that the problem is due the PECVD process sometimes inducing some changes in the local surface doping of the samples. Because changes in the doping level also produce a spectral shift, it becomes difficult in this situation to assess the part of the shift which is due to an effect of strain. At this point, we do not know the plasma conditions which induce this possible modification of the local surface doping.

3.2. μPL DOP

The DOP signal mesaured along the z direction (see figure 1) is defined [10] as $DOP_z = \dfrac{I_y - I_x}{I_x + I_y}$ where I_x is the component of the spectrally integrated PL signal with polarization parallel to the x axis of fig. 1. Cassidy et al. [10] have established that the DOP_z signal should be proportional to $(\epsilon_{xx} - \epsilon_{yy})$.
Note that the DOP informs us on the anisotropic part of the crystal deformation (perpendicular to the incident laser beam), contrary to the spectral shift which, as we have just explained, informs on the local volume change.
In this study, the DOP measurements were performed systematically along the z direction (i.e. parallel to the $< 100 >$ direction as shown in figure 1). Experimental DOP profiles across different SiN_x stripes on the InP surface can be seen in fig. 5. In this case the stripes were made from the film with maximum compressive built-in stress on InP (−250 MPa). The first thing to notice is that the DOP signal is weak (a few % maximum) but with a signal to noise ratio such that strains as small as 0.1% can be measured.

Sharp positive peaks appear on the DOP curves, especially on the outer stripe edges. Negative peaks can also be seen on the inner stripe edges. All these peaks are related to the strain concentration which is described within the edge force model by a divergence of the different strain coefficients [4]. Another interesting feature on fig. 5 is the DOP level in the central region of the different stripes which remains negative and never reaches zero. This observation clearly indicates that the crystal deformation is not isotropic even if this region is "far" away from the film edges like in the 100 μm stripe. The influence of the film

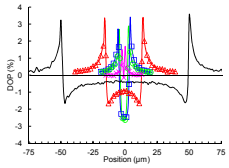

Figure 5: Measured DOP profiles for the compressive SiN_x layer on InP(100) with maximum stress, and stripes with different widths from 4 to 100 μm. Black full curve: $W = 100\,\mu$m; red curve with $\triangle$: $W = 30\,\mu$m; blue curve with $\square$: $W = 10\,\mu$m; green curve with $\bigcirc$: $W = 8\,\mu$m; pink curve with $\times$: $W = 4\,\mu$m.

edges can also be seen outside the stripes at distances more than 10 μm away from the edges where the DOP level remains slightly positive. This is certainly not an effect of the limited spatial resolution, in the order of 1 μm in our optical set-up. The DOP signal returns to zero outside the stripes – and far away from them – within the accuracy of our measurement technique.
DOP curves measured on a 100 μm stripe obtained from films with different built-in stresses are shown in fig. 6.

We can see that the sign of the DOP curves is inverted when the sign of the built-in stress changes. We can also see that the slope of the DOP curves in areas close to the film edges strongly changes with the magnitude of the built-in stress: for the stripes made from highly compressive films, the DOP peak has gradual sides, whereas it is very sharp for stripes made from low compressive films. Stripes on GaAs show the same trend (see fig. 7).

The DOP signal returns close to zero in the central region of the stripes only when the initial SiN_x has the lowest stress. This is the case for stripes on InP(100) and GaAs(100) substrates.

μPL DOP_z is a local measure of the difference in the normal deformation coefficients: $(\epsilon_{xx} - \epsilon_{yy})$. ϵ_{xx} is determined by the edge force within the edge force model and has the divergence already mentioned. However, ϵ_{yy} does not have a direct connection with the edge force model, as the edge force is directed along x [4]. Therefore ϵ_{yy} should be constant below the stripes, and zero outside. Some curvature measurements along a stripe, in the y direction, have been also performed, but no residual curvature could be detected. Consequently, as a first approximation, we considered ϵ_{yy} to be zero. Finite element simulations taking into account only the difference in the coefficients for thermal expansion for the SiN_x layer and for the substrate were carried for the different stripe widths. These simulations confirmed the assumption for ϵ_{yy}. Under this simplifying assumption, the DOP curves in figures 5 to 7 show the variations in ϵ_{xx} only, and a negative ϵ_{xx} (compression) should be associated to a positive DOP signal [10]. Based on this consideration, our DOP results show that a stripe etched in a film with compressive built-in stress induces, at the surface of the underlying substrate, compressive strain, perpendicular to the stripe length, outside the edges and tensile strain, perpendicular to the stripe length, between the edges.

4. Modelling

The last section covers the analytical model developped for discussing the μPL DOP results. This model should be applied to the μPL spectral shift measurements as well, but we have explained that we suspect these spectral shift measurements to be affected in some cases by local changes in the surface doping level induced by the PECVD process, in addition to the local strain effects.
The principle of the μPL DOP experiment is to measure the difference of the PL intensities with the two perpendicular polarizations, and then normalize this difference to the total PL signal. This allows us to compute a DOP signal from the following expression:

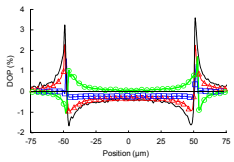

Figure 6: Measured DOP profiles for stripes with $W = 100\,\mu$m etched in SiN_x layers on InP(100) with different levels of built-in stress. Black curve: -250 MPa (compressive); red curve with $\triangle$: -200 MPa (compressive); blue curve with $\square$: -30 MPa (compressive); green curve with $\bigcirc$: 160 MPa (tensile).

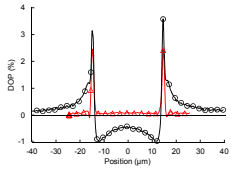

Figure 7: Measured DOP profiles for compressive SiN_x layers on GaAs(100), and stripe width 15 μm. Black curve with ◯: high compressive stress (−250 MPa); red curve with △: low compressive stress (−10 MPa).

$$DOP_{\mathrm{z}} = K \cdot \int_{z=0}^{\infty} (\epsilon_{\mathrm{xx}}(z) - \epsilon_{\mathrm{yy}}(z))\, e^{-\frac{z}{\alpha}} \mathrm{d}z \tag{1}$$

where K is a proportionality constant, and α is the absorption length in the substrate material. We assume that only the incident laser beam undergoes absorption, while the PL signal is not absorbed on its path to the sample surface. To take the limited spatial resolution into account, we should compute DOP_{z} at any spot x along the linescan and convolve with the resolution function (a gaussian profile). To save computing time, we have simply computed DOP_{z} with a step size of 0.5 μm and summed the signal at a given x location with the signal at the nearest neighbour locations (with a weighting factor) and the signal at the next-nearest neighbour locations (with a second weighting factor). The weighting factors have been calculated to reproduce the effect of the spatial resolution.

$\epsilon_{\mathrm{xx}}(z)$ in equation 1 will be deduced from the analytical formula given by the edge force model [4] for the stress tensor at any location (x, y, z) in the substrate. This model allows computing the stress tensor $\overline{\overline{\sigma}}(x, y, z)$ through the formulas:

$$\begin{aligned}
\sigma_{\mathrm{xx}} &= -\frac{2f}{\pi} \cdot \frac{(x+\frac{W}{2})^3}{[(x+\frac{W}{2})^2+z^2]^2} + \frac{2f}{\pi} \cdot \frac{(x-\frac{W}{2})^3}{[(x-\frac{W}{2})^2+z^2]^2} \\
\sigma_{\mathrm{yy}} &= 0 \\
\sigma_{\mathrm{zz}} &= -\frac{2f}{\pi} \cdot \frac{(x+\frac{W}{2}) \cdot z^2}{[(x+\frac{W}{2})^2+z^2]^2} + \frac{2f}{\pi} \cdot \frac{(x-\frac{W}{2}) \cdot z^2}{[(x-\frac{W}{2})^2+z^2]^2} \\
\sigma_{\mathrm{xy}} &= 0 \\
\sigma_{\mathrm{xz}} &= -\frac{2f}{\pi} \cdot \frac{(x+\frac{W}{2})^2 \cdot z}{[(x+\frac{W}{2})^2+z^2]^2} - \frac{2f}{\pi} \cdot \frac{(x-\frac{W}{2})^2 \cdot z}{[(x-\frac{W}{2})^2+z^2]^2} \\
\sigma_{\mathrm{yz}} &= 0
\end{aligned} \tag{2}$$

$f = \sigma_{\mathrm{f}} h$ with σ_{f} the built-in layer stress, h the layer thickness and W the stripe width (see fig. 1). The formulas in equation 2 have been obtained adding two edge-force contributions originating from opposite concentrated linear forces located at $x = \pm\frac{W}{2}$.

Assuming linear elasticity and taking the isotropic approximation for the strain-stress relations in the case of cubic crystals like GaAs or InP, the following formulas are used to derive the strain parameters ϵ_{xx} and ϵ_{yy} (although we specified the assumption allowing to consider ϵ_{yy} negligible we prefer to keep the formulas as general as possible):

$$\begin{aligned}
\epsilon_{\mathrm{xx}} &= \frac{1}{E}\left(\sigma_{\mathrm{xx}} - \nu\left(\sigma_{\mathrm{yy}} + \sigma_{\mathrm{zz}}\right)\right) \\
\epsilon_{\mathrm{yy}} &= \frac{1}{E}\left(\sigma_{\mathrm{yy}} - \nu\left(\sigma_{\mathrm{xx}} + \sigma_{\mathrm{zz}}\right)\right)
\end{aligned} \tag{3}$$

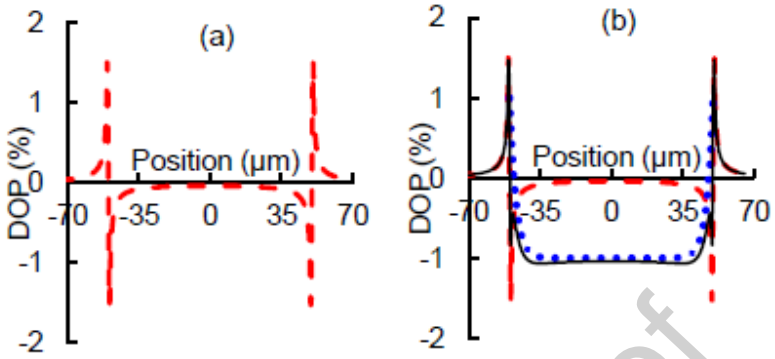

Figure 8: Example of calculated DOP profiles: a : taking into account only the edge force model (red dashed curve); b : taking into account the edge force model (red dashed curve) and the internal anisotropic strain with exponential relaxation near the edges (blue dotted curve); the black curve (full line) on b is the total calculated DOP.

where E and ν are the Young's modulus and Poisson's ratio.
Equation 1 becomes:

$$DOP_z = K \cdot \frac{1-\nu}{E}\frac{2f}{\pi}\int_{z=0}^{\infty}\Big[\frac{(x-\frac{W}{2})^3}{[(x-\frac{W}{2})^2+z^2]^2} - \frac{(x+\frac{W}{2})^3}{[(x+\frac{W}{2})^2+z^2]^2}\Big]e^{-\frac{z}{\alpha}}\mathrm{d}z \tag{4}$$

The quantity $K \cdot \frac{1-\nu}{E}\frac{2f}{\pi}$ is denoted A in the following. Using this procedure, with an arbitrary value for the parameter A, we obtain the curve displayed in fig. 8–a. This curve cannot reproduce the experimental DOP profiles, mainly for three reasons:

- the DOP is zero in the central area;
- the magnitudes of the positive and negative peaks at each edge are the same (in fact the edge force model yields ϵ_{ii} which are all antisymmetric with respect to x variations across the location of the singularity); and,
- there is no parameter at this stage in the model allowing a control of the slope of the DOP curves in areas close to the film edges.

In order to correct for the first point, we simply add a parameter to include some residual anisotropy in the central part of the stripes, where the influence of the edge forces becomes negligible. This parameter is denoted B. We add B to DOP_z calculated from eq. 4 when x corresponds to locations below the

Parameter	Fixed / Adjusted
A $\left(= K \cdot \frac{1-\nu}{E} \frac{2\sigma_{\mathrm{f}} \cdot h}{\pi}\right)$	Adjusted
B (DOP in center part of stripe)	Adjusted
C (edge relaxation – additional contribution to DOP at edges)	Adjusted
D (length scale for edge relaxation of DOP)	Adjusted
α (absorption length in GaAs or InP)	Fixed
Weight affected to nearest and next-nearest neighbour points – finite spatial resolution (2 parameters)	Fixed

Table 1: Parameters used in the analytical model

stripe ($-\frac{W}{2} < x < \frac{W}{2}$). Then to cover the other two inconsistancies, we considered that the SiN_x stripes may undergo some stress relaxation near the edges. This effect was included into our model by adding an exponentially varying contribution to the DOP_{z} signal from eq. 4. This additional contribution is controlled by introducing two parameters: C and D corresponding respectively to the value added to the edge-force DOP_{z} to include this edge relaxation and to the lengthscale of this relaxation effect.
Similar to the residual anisotropy, this exponential relaxation is taken into account only for x values below the stripe ($-\frac{W}{2} < x < \frac{W}{2}$). Figure 8–b illustrates qualitatively the modifications to the basic edge-force DOP model allowed by these two additional physical contributions. The modifications shown in fig. 8–b yield a DOP that is consistent with experimentally obtained results, as shown in figs. 5 to 7. Table 1 summarizes the parameters governing our DOP analytical model: 4 adjustable parameters are allowed to vary during the fitting procedure to the experimental DOP curves, 3 parameters are kept fixed.
A is related to the built-in stress. B accounts for the residual anisotropy (i.e., the deformation below stripes with a large aspect ratio – width strongly different from length – cannot be considered biaxial as below an infinite film). C and D characterize some relaxation of the stress near the edges, with exponential variation (it is important to consider that this contribution may simply reduce

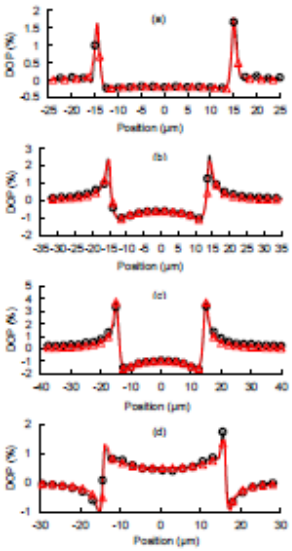

Figure 9: Adjustement of the model to experimental DOP profiles for SiN_x stripes ($W = 30\mu$m) etched from layers grown on InP(100) with the different built-in strains. Black curve with ◯: experimental data; red curve with △: model. (a) −30 MPa; (b) −200 MPa; (c) −250 MPa; (d) +160 MPa.

the magnitude of DOP_z near the stripe edges or even change locally its sign as shown on fig. 8–b). The contributions controlled by parameters B, C and D should in principle be made dependent on the depth coordinate z (as is the case for the edge force model). Anyhow, to keep the number of adjustable parameters limited – and also because we have no knowledge of how these variations should be written – we did not take this into account at the moment.
Figure 9 shows the efficiency of this analytical model to fit our experimental DOP curves, for SiN_x stripes made from layers grown on InP(100) with different built-in strains. These best fit curves are in good agreement with the DOP profiles in all cases. A similar good agreement was obtained for all the GaAs(100) and InP(100) samples which were measured. As an illustration of the trends which can be extracted from the μPL DOP linescans and associated fits with the analytical model, fig. 10 displays the evolution of the A parameter (linked to the edge force) versus built-in strain for the SiN_x layers grown on InP(100). Each curve in fig. 10 corresponds to a different stripe width. From the results in fig. 10 one can deduce that the magnitude of the edge force does not appear to be determined uniquely by the initial built-in strain. Instead, values for A as obtained from linear best fits indicate that for a given built-in strain the edge force decreases as the stripe width decreases. This is a second – indirect – evidence that there is some stress relaxation. This stress relaxation is

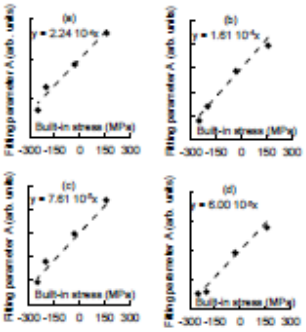

Figure 10: Fitting parameter A determined from the adjustement of the model to the experimental DOP profiles for SiN_x layers grown on InP(100) with the different built-in strains. (a) stripe width $W = 100\,\mu$m; (b) $W = 30\,\mu$m; (c) $W = 10\,\mu$m; (d) $W = 8\,\mu$m. Black dots: A parameter obtained from each fit; dashed line: linear best fit to the values obtained for A. The coefficient for the best fit line is also indicated for each case.

more significant for narrower stripes. Going from $W = 100\,\mu$m to $W = 8\,\mu$m, the magnitude of the edge force seems to be reduced by 75 % approximately. Finally we show in fig. 11 the trend for the fitting parameter B, which simply represents the residual DOP signal measured in the central area of each stripe. The results in this figure show that the residual anisotropic deformation at the stripe center increases for decreasing stripe width. The best fit parameters for this quantity indicate that the anisotropic deformation is much more dependent on the built-in stress for narrow stripes than for larger stripes.

5. Discussion

We have shown a procedure to perform analysis of the strain induced in InP or GaAs substrates by the presence of thin film dielectric stripes with different levels and signs of the built-in strain. The built-in strain in these films derives from the parameters controlling the PECVD process. By combining two different implementations of μPL set-ups (spectral shift and DOP of the spectrally integrated signal) we are able, in principle, to get scan or maps of both the local volume change and anisotropic deformation in the substrates, under the influence of the dielectric stripe. Anyhow, we have observed that the spectral shift of the PL line may be affected, in some of our experiments, by another factor than the local strain. Our assumption of a change in the surface doping of the semiconductor related to the reactants from the PECVD reactor has to be confirmed by further experiments. In this paper, we focussed on a careful analysis of the μPL DOP linescans. Starting from the basic edge force model, we built step-by-step an analytical model which allows accurate fitting of our experimental DOP data with a limited set of adjustable parameters. These parameters have a physical meaning for the strain distribution in the underlying

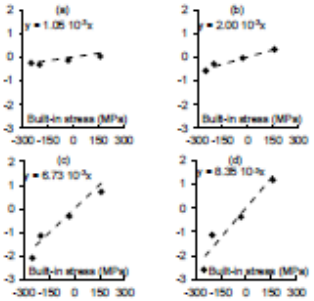

Figure 11: Fitting parameter B (residual DOP - in %) determined from the adjustement of the model to the experimental DOP profiles for SiN_x layers grown on InP(100) with the different built-in strains. (a) stripe width $W = 100\,\mu$m; (b) $W = 30\,\mu$m; (c) $W = 10\,\mu$m; (d) $W = 8\,\mu$m. Black dots: B parameter obtained from each fit; dashed line: linear best fit to the values obtained for B. The slope for the best fit line is also indicated for each case.

substrate (magnitude of the effective edge force, residual anisotropic deformation in the central area, magnitude and lengthscale of the stress relaxation at the edges).

The original edge force model [4] appears insufficient to describe the measured strain distribution: it does not account for the observed residual anisotropy, it does not reproduce the relative magnitude of the strain peaks on both sides of film edges, and it does not either allow for a control of slopes of the decreasing deformation near film edges. Using our modified model, we can reproduce in a satisfactory way the experimental μPL DOP linescans for all our samples, using a limited number of adjustable parameters. The trends for these fitting parameters (especially the effective edge force parameter A and the DOP residual anisotropy parameter B) are a first step towards a quantitative description of the strain / stress effects in these samples, and additionally bring some insight into the different physical effects which could have an impact on this issue. We observe a decrease of the effective edge force parameter A, for a given level and sign of the initial built-in stress, when the stripe width decreases. This decrease is attributed to some strain relaxation near the edges of the film. In our model, we chose to assume that this strain relaxation has an exponential dependence on the distance to the edge to take into account the strong changes on the slopes of the DOP curves which we observed. We point out that this problem of strain relaxation at the edges of a discontinuous thin film on a substrate was already discussed in the framework of an extension of the original "concentrated edge force" model by Hu[18] where the problem of the stress step at the film edge was treated self-consistently. The stress step resulting from the simple edge force assumption (film stress perpendicular to the edge shifts abruptly from the built-in value to zero) is removed by considering a distributed edge force and a partial stress relaxation. This strain relaxation issue at the edges of thin films on substrates was also at the heart of the finite element simulation work by Jain

et al. [7, 8]. Having an accurate description of the local strain in components such as photonic devices (waveguides especially) is of the highest importance because of the photoelastic effect [19] which can modify the optical properties and introduce birefringence.

The model described in this paper is only semi-quantitative, it does not yield a full calculation of the local stress or strain tensor at any location of the substrate. One of the problems to solve is the determination of the constant relating DOP to elements of the strain tensor. D.T. Cassidy et al. [10] have determined a "DOP constant" C_{DOP} such that $DOP_{\mathrm{y}} = -C_{\mathrm{DOP}}\,(\epsilon_{\mathrm{xx}} - \epsilon_{\mathrm{zz}})$. The measurements were done along the $< 110 >$ direction of cleaved facets, and yield $C_{\mathrm{DOP}} = 65 \pm 10$ for InP(110) and $C_{\mathrm{DOP}} = 50 \pm 10$ for GaAs(110). These formula assume that ϵ_{xx} and ϵ_{zz} do not have any y dependence. Assuming that the same calibration constants are valid for the geometry used in the present study (DOP measurements along the $< 100 >$ direction), one would get (following Landesman et al. [20]) $K = \dfrac{C_{\mathrm{DOP}}}{\alpha}$. Our fitting parameter A would then write as $A = \dfrac{C_{\mathrm{DOP}}}{\alpha}\dfrac{1-\nu}{E}\dfrac{2\sigma_{\mathrm{f}}.h}{\pi}$. Taking the following numerical values for InP:

$\alpha = 150$ nm

$\nu = 0.292$

$E = 60.9$ GPa

the fitting parameter would then be $A = 5.68 \cdot 10^{-4}\sigma_f(MPa)$. Comparing with the linear best fit equations in fig. 10, this indicates values for the effective edge force of $\sim 40\%$ of that predicted by the simplest edge force model without relaxation for $W = 100\,\mu$m and $\sim 10\%$ for $W = 8\,\mu$m.

An improvement direction for our model is to include some z dependence for the residual anisotropy and edge relaxation. As already pointed out, this dependence was not included at this stage because of a lack of knowledge on how the z variation should be and the necessity to keep the number of adjustable parameters to a limited set. We plan to investigate this question by performing some scannings and mappings on cleaved cross sections of the samples. As shown previously [14] this type of measurement provides valuable insight into the spatial variation of the different coefficients of the strain tensor, provided an accurate and good quality cleavage surface can be obtained in the area below a SiN_x stripe.

Our procedure for the measurement of strain profiles below thin dielectric stripes should prove very useful in the context of development and process optimization of photonic devices, especially in two different approaches. First, as already mentioned, stress/strain due to these thin films modifies the optical performance in components such as waveguides. It is therefore of the highest importance to have the best possible description of stress/strain distribution in and around the key regions in such devices. Second, once the effects are precisely understood and described, it is sometimes possible to make use of these effects to design specific devices and components such as photoelastic waveguides [21]. We think this procedure could also be useful in a "process control" approach, as a sensitive method to check the reproducibility of the thin films produced and process

parameters employed to shape these thin films.

6. Conclusion

The general goal of the work was to investigate the details of the strain/stress field generated in GaAs(100) and InP(100) substrates by the presence of SiN_x stripes of different widths, fabricated from PECVD films with well-controlled built-in stress. We used two implementations of the μPL technique to measure the local strain, with the idea to get both the local volume change (from the spectral shift) and anisotropic deformation (from the DOP). The spectral shift measurements show very high sensitivity to the local isotropic strain. Some PECVD conditions yield an additional component to the local spectral shift with noisy spatial variation, which hinders a proper determination of the isotropic strain. We think that the origin of this additional component is an effect of the PECVD molecules, ions, and radicals on the local surface doping. Because of this effect, we were not able to perform a systematic study of the isotropic strain distribution through the μPL-spectral shift technique. We need to identify which PECVD conditions yield this modification of the surface doping and explain the effects.

On the other hand, the DOP technique was revealed to be sensitive to the local anisotropic strain, and to be immune to PECVD effects on the sample surface. We obtained DOP profiles for the different PECVD conditions and stripe widths which showed interesting trends. The DOP curves show in particular sharp peaks near the stripe edges. These peaks are caused by the strain concentration on both sides of each stripe edge, which has been described in the literature through the concept of the concentrated edge force. The DOP signal returns to zero outside the stripes, with decreasing length and abrupness which seem to change strongly with the PECVD conditions. Inside the stripes, the DOP signal does not always return to zero below the central stripe area, even for the largest stripes. This indicates some residual anisotropic deformation.

In order to extract quantitative information from the DOP profiles, we built an analytical model which is described step by step. This model starts with the formulas given by the concentrated edge force model, adding two contributions: one to account for the residual anisotropic deformation in the central part of the stripes, and another one which describes some strain relaxation occuring close to the edges. We noticed that this edge relaxation was already introduced in the literature through the "distributed edge force" concept. Using this model, in an effort to restrict the number of adjustable parameters, we obtained good fits to all our experimental data. Looking at the trends for the different fitting parameters, we showed that this approach produces information on the behaviour of the different samples which seems coherent with the PECVD conditions used and stripe geometry.

Altogether, we think that the type of data produced can be very efficient for the development and optimization of photonic devices where mechanical stress can play an important role through the photo-elastic effect, such as for optical waveguides and multi-mode interference components. The measurements and

simulations can be helpful in a process control approach, to check the reproducibility of the thin film growth and processing conditions.
The analytical model needs some improvement. In particular, the depth dependence of the residual anisotropy and edge relaxation effect were not taken into account. We plan to introduce this dependence. In order to evaluate the trends, more measurements are needed, such as μPL-DOP maps measured from cleaved (110) cross sections immediately below a stripe. These measurements are under way. An accurate finite element simulation approach, taking into account all the details revealed in this study, will also be developed to provide validation of the simple analytic model and useful technical information in the context of device design and optimization.

7. Acknowledgements

Part of the samples were prepared in the technology platform Nano-Rennes. The μPL spectral shift measurements were made on equipment from the ScanMAT platform. Both plaforms are sponsored by the University of Rennes-1 and the CNRS.

References

[1] M. Huang, Stress effects on the performance of optical waveguides, International Journal of Solids and Structures 40 (2003) 1615–1632.

[2] A. R. Adams, Strained-Layer Quantum-Well Lasers, IEEE Journal of Selected Topics in Quantum Electronics 17 (2011) 1364–1373.

[3] G. G. Stoney, The Tension of Metallic Films Deposited by Electrolysis, Proceedings of the Royal Society A: Mathematical, Physical and Engineering Sciences 82 (1909) 172–175.

[4] S. M. Hu, Film-edge-induced stress in silicon substrates, Applied Physics Letters 32 (1978) 5–7.

[5] G. Abadias, E. Chason, J. Keckes, M. Sebastiani, G. B. Thompson, E. Barthel, G. L. Doll, C. E. Murray, C. H. Stoessel, L. Martinu, Review Article: Stress in thin films and coatings: Current status, challenges, and prospects, Journal of Vacuum Science & Technology A: Vacuum, Surfaces, and Films 36 (2018) 020801/1–020801/48.

[6] C. E. Murray, Mechanics of edge effects in anisotropic thin film/substrate systems, Journal of Applied Physics 100 (2006) 103532/1–103532/9.

[7] S. C. Jain, A. H. Harker, A. Atkinson, K. Pinardi, Edge-induced stress and strain in stripe films and substrates: A two-dimensional finite element calculation, Journal of Applied Physics 78 (1995) 1630–1637.

[8] S. C. Jain, M. Willander, H. Maes, Stresses and strains in epilayers, stripes and quantum structures of III–V compound semiconductors, Semiconductor Science and Technology 11 (1996) 641–671.

[9] J. Jimenez, J. W. Tomm, Spectroscopic Analysis of Optoelectronic Semiconductors, volume 202 of *Springer Series in Optical Sciences*, Springer International Publishing, Cham, 2016. URL: http://link.springer.com/10.1007/978-3-319-42349-4. doi:10.1007/978-3-319-42349-4.

[10] D. T. Cassidy, S. K. K. Lam, B. Lakshmi, D. M. Bruce, Strain mapping by measurement of the degree of polarization of photoluminescence, Applied Optics 43 (2004) 1811–1818.

[11] J. A. Taylor, The mechanical properties and microstructure of plasma enhanced chemical vapor deposited silicon nitride thin films, Journal of Vacuum Science & Technology A: Vacuum, Surfaces, and Films 9 (1991) 2464–2468.

[12] P. A. Flinn, Principles and Applications of Wafer Curvature Techniques for Stress Measurements in Thin Films, MRS Proceedings 130 (1988) 41.

[13] J.-P. Landesman, Micro-photoluminescence for the visualisation of defects, stress and temperature profiles in high-power III–V's devices, Materials Science and Engineering: B 91-92 (2002) 55–61.

[14] J.-P. Landesman, D. T. Cassidy, M. Fouchier, C. Levallois, E. Pargon, N. Rochat, M. Mokhtari, J. Jiménez, A. Torres, Mapping of mechanical strain induced by thin and narrow dielectric stripes on InP surfaces, Optics Letters 43 (2018) 3505–3508.

[15] F. H. Pollak, M. Cardona, Piezo-Electroreflectance in Ge, GaAs, and Si, Physical Review 172 (1968) 816–837.

[16] M. Neuberger, III-V Semiconducting Compounds, Springer US, Boston, MA, 1971. URL: https://doi.org/10.1007/978-1-4615-9606-6, oCLC: 851731806.

[17] D. E. Aspnes, A. A. Studna, Dielectric functions and optical parameters of Si, Ge, GaP, GaAs, GaSb, InP, InAs, and InSb from 1.5 to 6.0 eV, Physical Review B 27 (1983) 985–1009.

[18] S. M. Hu, Film-edge-induced stress in substrates, Journal of Applied Physics 50 (1979) 4661–4666.

[19] Z. H. Levine, H. Zhong, S. Wei, D. C. Allan, J. W. Wilkins, Strained silicon: A dielectric-response calculation, Physical Review B 45 (1992) 4131–4140.

[20] J.-P. Landesman, D. T. Cassidy, J. W. Tomm, M. L. Biermann, Strain measurement, in: J. W. Tomm, J. Jiménez (Eds.), Quantum-Well Laser Array Packaging, McGraw Hill Nanoscience, McGraw-Hill Companies, New York, NY, 2007.

[21] W. Ye, D.-X. Xu, S. Janz, P. Cheben, M.-J. Picard, B. Lamontagne, N. Tarr, Birefringence control using stress engineering in silicon-on-insulator (SOI) waveguides, Journal of Lightwave Technology 23 (2005) 1308–1318.

Declaration of Competing Interest

The authors declare that they have no known competing financial interests or personal relationships that could have appeared to influence the work reported in this paper.

Credit author statement

Solène Gérard : Investigation, Validation, Formal analysis, Software, Writing - Original Draft, Visualization

Merwan Mokhtari : Investigation, Formal analysis

Jean-Pierre Landesman : Conceptualization, Methodology, Software, Writing - Original Draft, Supervision, Project administration

Christophe Levallois; Methodology, Investigation, Resources, Writing - Review & Editing

Marc Fouchier: Investigation, Methodology

Erwine Pargon: Investigation, Resources, Writing - Review & Editing

Philippe Pagnod-Rossiaux: Investigation, Resources

François Laruelle: Investigation, Resources

Alain Moréac: Investigation, Formal analysis

Brahim Ahammou: Investigation

Daniel T. Cassidy : Writing - Review & Editing, Conceptualization